The buoyancy-driven motion of a single skirted bubble or drop rising through a viscous liquid

Cite as: Phys. Fluids **24**, 112101 (2012); https://doi.org/10.1063/1.4765669
Submitted: 01 November 2011 . Accepted: 03 October 2012 . Published Online: 12 November 2012

Mitsuhiro Ohta, and Mark Sussman

The buoyancy-driven motion of a single skirted bubble or drop rising through a viscous liquid

Mitsuhiro Ohta[1,a)] and Mark Sussman[2]
[1]*Division of Applied Sciences, Graduate School of Engineering, Muroran Institute of Technology, 27-1 Mizumoto-cho, Muroran, Hokkaido 050-8585, Japan*
[2]*Department of Mathematics, Florida State University, Tallahassee, Florida 32306, USA*

(Received 1 November 2011; accepted 3 October 2012; published online 12 November 2012)

The buoyancy-driven motion of a single skirted bubble or drop rising through a viscous liquid is computationally explored by way of 3d-axisymmetric computations. The Navier-Stokes equations for incompressible two-fluid flow are solved numerically in which the coupled level-set and volume-of-fluid method is used to simulate the deforming bubble/drop boundary and the interface jump conditions on the deforming boundary are enforced through a sharp interface numerical treatment. Dynamic, block structured adaptive grid refinement is employed in order to sufficiently resolve the thin skirts. Results on the sensitivity of the thickness of trailing bubble/drop skirts to the density ratio and viscosity ratio are reported. It is shown that both the density ratio (not the density difference) and the viscosity ratio effect the skirt thickness. Previous theory for predicting skirt thickness can be refined as a result of our calculations. It is also discovered that the formation of thin skirts for bubbles and drops have little effect on the rise velocity. In other words, the measured *Re* number for cases without skirt formation have almost the same values for *Re* as cases with a thin skirt. © *2012 American Institute of Physics*. [http://dx.doi.org/10.1063/1.4765669]

I. INTRODUCTION

In medium Morton number (M) ($10^{-1} < M < 10^4$) and large Eötvös number (Eo) conditions ($200 < Eo$), and with a Reynolds number (Re) of the order 10 to 100, buoyantly rising spherical-cap bubbles and drops might possess an attached, trailing thin gas/liquid film (a "skirt"). The dynamics of skirted bubbles and drops is a field not only interesting in terms of unique fluid mechanics, but also having direct applications in gas-liquid and liquid-liquid reactors. The presence of skirts on a bubble or drop effects the heat and mass transfer characteristics around the bubble (drop) and effects the flow behind the bubble (or drop).[1] The study of bubble dynamics in general, not only the study of skirted bubbles, has applications in "many bubble systems." Gupta and Kumar[2] numerically studied many bubble systems in order to further understand boiling and two-phase flow in micro-mini channels. For studying many bubble systems, a numerical method for computing many bubbles will inevitably be confronted with an "under-resolved grid" and it is important to understand the behavior of numerical methods, when the grid is *not* resolved. For example, a "smeared interface method" for numerically simulating the transition region from gas to liquid[3] will artificially predict skirted bubbles with relatively thick skirts when the grid is under-resolved, on the other hand, a sharp interface method[4] predicts a skirt that is too thin on an under-resolved grid *but* nonetheless captures the overall bubble dynamics much better than the "smeared interface" approach. We find, computationally using a sharp interface method, that the bubble dynamics with a very thin skirt is very similar to that of a bubble with no skirt.

[a)]Present address: Department of Energy System, Institute of Technology and Science, The University of Tokushima, 2-1 Minamijyousanjima-cho, Tokushima 770-8506, Japan. Electronic mail: m-ohta@tokushima-u.ac.jp.

As early as 1885, Thomson and Newall[5] reported observations of a falling skirted drop. Other reports on the motion of skirted bubbles and drops have been provided by Shoemaker and Marc De Chazal[6] (drop), Wairegi[7] (drop), Wairegi and Grace[8] (drop), Bhaga[1] (drop), Angelino[9] (bubble), Davenport *et al.*[10] (bubble), Guthrie and Bradshaw[11,12] (bubble), Calderbank *et al.*[13] (bubble), Wegener *et al.*[14] (bubble), Wairegi[7] (bubble), Bhaga[1] (bubble), and Hnat and Buckmaster[15] (bubble). The majority of previous experimental studies on skirted bubbles and drops do not report on the sensitivity of the skirt thickness with respect to physical properties and bubble/drop size. The following experimental work on skirted bubbles and drops are exceptions in which more detailed information on skirted bubbles/drops were reported: Guthrie and Bradshaw,[11,12] Wairegi,[7] Bhaga,[1] and Hnat and Buckmaster.[15]

Guthrie and Bradshaw[11] experimentally measured the skirt thickness behind bubbles and reported that skirts had a $27 \sim 55$ μm thickness. Whereas the thickness of gas skirts is extremely thin, the skirts trailed behind drops were found to be of the order 1 mm in thickness (Wairegi[7] and Bhaga[1]). Experimental results show that the skirt thickness of drops is much thicker than that for bubbles. Guthrie and Bradshaw[11] estimated the skirt thickness of a bubble using a guillotine technique. In order to obtain the volume of the skirt part trailed behind the bubble, the skirt was chopped off from the main body of the bubble by instantaneously inserting a thin steel plate across an experimental column. At the same time, they calculated the interfacial surface area of the skirt using photographic measurements. The accuracy of determination of the skirt thickness was within $\pm 30\%$ according to Guthrie and Bradshaw. Wairegi[7] and Bhaga[1] calculated the skirt thickness as a function of position by means of photographic measurements with a refractive index correction. The procedure taken by Wairegi[7] and Bhaga[1] enabled them to report how the skirt thickness depends on position as a bubble rises.

From their experimental results, Guthrie and Bradshaw[11] developed a theoretical model for predicting skirt thickness of a skirted bubble based on physical properties of the gas and liquid and the bubble size. Wairegi[7] extended the work of Guthrie and Bradshaw[11] by deriving a theoretical expression for predicting skirt thickness of skirted drops as well as skirted bubbles. The work of Wairegi[7] was further extended by Bhaga[1] who introduced a shape dependent thickness coefficient and a correction factor for deviation from potential flow in order to derive an even more sophisticated model for predicting skirt thickness.

In this paper, we study skirted bubbles and drops computationally. The deforming bubble/drop boundary is numerically represented by the coupled level set and volume of fluid (CLSVOF) method and the interfacial boundary conditions are numerically enforced using a sharp interface approach.[4,16,17] A numerical method enables one to analyze the pressure field, vorticity, skirt thickness, and streamlines much more readily than an experimental approach. Also, with a numerical method, it is very easy to vary parameters in order to develop even more precise theoretical models for predicting skirt thickness. The objective of our study is to examine the sensitivity of the thickness of a buoyantly rising bubble/drop skirt for varying density and viscosity ratios. We believe that this is the first time that one has used a numerical method to examine the sensitivity of skirt thickness due to varying physical properties of the liquid and gas, and the size of the buoyantly rising bubble/drop. Previous studies of skirt thickness have been experimental studies. Our results show that the theory on skirt thickness developed by Bhaga[1] can be further refined with an added dependence on the density ratio λ.

We remark that for our numerical study of skirt thickness, we model the transition region from gas to liquid to be perfectly sharp.[4,16,17] Our algorithm is in contrast to previous work on the numerical simulation of buoyantly driven motion of skirted bubbles or drops,[2,3,18–35] which effectively give the gas/liquid interface a numerical thickness of at least one grid cell thickness. A "smeared interface method" requires a much higher grid resolution than a sharp interface method in order to resolve skirted bubble/drop flow. Numerical methods which artificially give the interface a thickness effectively increase the bubble (drop) viscosity at the rim of a rising bubble (drop). As instructed by the theoretical models of Guthrie and Bradshaw,[11] the skirt thickness is proportional to the viscosity of the bubble (drop). Guthrie and Bradshaw[11] experimentally produced bubbles with a very small skirt thickness of about $27 \sim 55$ μm. On the other hand, the skirted bubbles computed by previous practitioners, in which *Eo*, *Re*, and *M* fall in the skirted bubble region specified by Bhaga

TABLE I. List of recent work that report results for numerically simulating skirted bubbles and drops. The algorithm used by each paper artificially gives the interface a thickness of at least one grid cell.

Authors	Interface representation	Skirted bubbles/drops
Unverdi and Tryggvason[18]	Front-Tracking method (FT)	Bubbles
Sussman and Smereka[19]	Levelset method (LS)	Bubbles
Ohta and Suzuki[20]	Volume-of-Fluid method (VOF)	Drops
Ohta *et al.*[21]	Coupled LS and VOF method (CLSVOF)	Bubbles
Inamuro *et al.*[22]	Lattice Boltzmann Method (LB)	Bubbles
Ohta *et al.*[3]	CLSVOF	Bubbles
van Sint Annaland *et al.*[23]	VOF	Bubbles
van Sint Annaland *et al.*[24]	FT	Bubbles
Bonometti and Magnaudet[25]	VOF	Bubbles
Hua and Lou[26]	FT	Bubbles
Hua *et al.*[27]	FT	Bubbles
Gupta and Kumar[2]	LB	Bubbles
Yu and Fan[28]	LS	Bubbles
Yu and Fan[29]	LB	Bubbles
Wang *et al.*[30]	CLSVOF	Bubbles
Hysing *et al.*[31]	LS and VOF	Bubbles
Amaya-Bower and Lee[32]	LB	Bubbles
Farhat *et al.*[33]	LB	Bubbles
Pianet *et al.*[34]	VOF	Bubbles
Krishnan *et al.*[35]	VOF	Bubbles

and Weber[36] and the density ratio is on the order of 1000 to 1, possessed a skirt with a thickness on the order of 1 mm, which corresponds to a skirted *drop* rather than a skirted *bubble*. We also note that some researchers (see, e.g., Ref. 33) numerically study bubble motion using a density ratio that is much smaller than the density ratio of water to air. We find in this paper that decreasing the density ratio, keeping all other dimensionless groups fixed, increases the skirt thickness. We have tabulated previous work on the numerical simulations of skirted bubbles and/or drops in Table I.

II. MATHEMATICAL FORMULATION

A. Governing equations

We make the assumption that the liquid/liquid or liquid/gas flow is isothermal, Newtonian, and incompressible. The density in each fluid is constant. The interface separating the deforming boundary is an immiscible interface. We shall also assume that the skirted bubble/drop motion is axis-symmetric; i.e., we shall compute skirted bubble/drop motion in a cylindrical coordinate system in which all the variables are independent of θ and the velocity in the azimuthal direction is zero.

The mass conservation equation simplifies to the incompressibility constraint,

$$\nabla \cdot \boldsymbol{u} = 0, \tag{1}$$

where $\boldsymbol{u} = (u, v, w)$ is the fluid velocity. The time evolution of the two-phase flow is governed by the incompressible Navier-Stokes equations with the one-fluid formulation form based on the CLSVOF method for representing the deforming interface,

$$\frac{\partial \boldsymbol{u}}{\partial t} + (\boldsymbol{u} \cdot \nabla)\boldsymbol{u} = \frac{1}{\rho}\nabla \cdot (-p\boldsymbol{I} + 2\mu \boldsymbol{D}) + \boldsymbol{g} - \frac{\sigma\kappa}{\rho}\nabla H. \tag{2}$$

t is the time, p is the pressure, $\boldsymbol{I}$ is the unit tensor, and $\boldsymbol{D}$ is the rate-of-deformation tensor defined by $2\boldsymbol{D} = \nabla \boldsymbol{u} + (\nabla \boldsymbol{u})^T$. $\boldsymbol{g}$ is the gravitational acceleration, κ is the curvature of the interface, σ denotes the (constant) surface tension coefficient, and H is the Heaviside function (see Eq. (4)).

Since ρ and μ are constant in each fluid with a jump at the interface, they are defined as

$$\rho = \rho_B(1-H) + \rho_S H, \qquad \mu = \mu_B(1-H) + \mu_S H. \tag{3}$$

In (3), the subscripts "B" and "S" denote "bubble/drop" and "suspending fluid," respectively. H is a function of the level-set (LS) function (ϕ) and is defined as follows:

$$H = \begin{cases} 1 & \phi \geq 0 \\ 0 & \phi < 0 \end{cases}. \tag{4}$$

Since the free surface is represented by the CLSVOF method, equations for the time evolution of the volume-of-fluid (VOF) function F and the level-set (LS) function ϕ are needed too

$$\frac{\partial F}{\partial t} + (\boldsymbol{u}\cdot\nabla)F = 0, \tag{5}$$

$$\frac{\partial \phi}{\partial t} + (\boldsymbol{u}\cdot\nabla)\phi = 0. \tag{6}$$

The term $\sigma\kappa$ in (2) corresponds to the surface tension-induced jump in the normal stress. The singular source term in the right hand side of the Navier-Stokes equation, $\frac{\sigma\kappa}{\rho}\nabla H$, is equivalent to specifying that the jump in the normal stress is $\sigma\kappa$. Weak solutions of the one-fluid formulation satisfy the interface jump conditions;[37] analogously, numerical solutions of our sharp interface discretization of the one-fluid formulation (see Sec. II B), will also satisfy the interface jump conditions.[16] There is no need to explicitly enforce jump conditions at the deforming boundary.

We non-dimensionalize (1) and (2) by assuming d (the volume-equivalent diameter of a bubble or drop) as a characteristic length scale and U_T (the terminal rise velocity) as a characteristic velocity scale. Introducing a dimensionless length $x^* = x/d$ ($x^* = x/d$), a dimensionless velocity $u^* = u/U_T$, a dimensionless time $t^* = t/(d/U_T) = U_T t/d$, a dimensionless curvature $\kappa^* = \kappa/(1/d) = d\kappa$, we derive the non-dimensionalized mass conservation equation and the non-dimensionalized Navier-Stokes equations. Hereinafter, we show the dimensionless governing equations with omission of the asterisk for the sake of simplicity

$$\nabla\cdot\boldsymbol{u} = 0, \tag{7}$$

$$\frac{\partial \boldsymbol{u}}{\partial t} + (\boldsymbol{u}\cdot\nabla)\boldsymbol{u} = \frac{1}{\rho}\nabla\cdot(-p\boldsymbol{I} + \frac{1}{Re}\mu(\nabla\boldsymbol{u} + \nabla\boldsymbol{u}^T)) + \frac{1}{Fr}\hat{z} - \frac{\kappa}{\rho}\frac{1}{We}\nabla H. \tag{8}$$

The density and viscosity are now defined by dimensionless form

$$\rho = \lambda(1-H) + H\mu = \eta(1-H) + H. \tag{9}$$

In Eqs. (8) and (9), Re ($=\rho_S U_T d/\mu_S$) is the Reynolds number, We ($=\rho_S U_T^2 d/\sigma$) is the Weber number, Fr ($=U_T^2/gd$) is the Froude number defined in this study, and this form can be related by $Fr = Fr_o^2$ using the ordinal Froude number Fr_o ($=U_T/\sqrt{gd}$). $\hat{z}$ is a unit downward pointing vector. Another dimensionless parameter that appears above is the dimensionless pressure, $p = p/(\rho_S U_T^2)$. From the formulation in Eqs. (7)–(9), one observes that bubble/drop dynamics can be completely determined by Re, We, Fr, λ, and η.

Remarks:

- We assume that the density is constant in the buoyantly rising bubble/drop. For the parameter sets that we have used, we find that the pressure in the bubble/drop varies only slightly (the reduced pressure field is illustrated in Figures 7 and 9). We do not think the pressure variations that we have observed are enough that we would have to consider the effect of compressibility in the bubble/drop on our sensitivity study of skirted bubble/drop flow.
- For the purpose of examining the sensitivity of skirted bubble/drop dynamics with respect to varying density and viscosity ratio, we think it is ok to assume axis-symmetry for skirted bubbles and drops. For skirted bubble rise motion, the values for M and Eo that we consider fall in the "skirted with smooth, steady skirt" region defined by Bhaga and Weber.[36]

B. Numerical method

We simulate the buoyancy-driven motion of a skirted bubble/drop through a viscous liquid using a sharp interface,[4,16,17,38] CLSVOF[39,40] method for incompressible two-phase flow. The advantage of a sharp interface method,[4,16,17,38] as opposed to a smeared interface method[41] is that a sharp interface method does not require as much resolution within a skirt as a smeared interface method. It is also easier to establish convergence with a sharp interface method because we do not have to verify that our results are insensitive to smearing parameters. In our computations, the spatial discretization of Eqs. (7) and (8) is a second-order finite difference approximation within the bulk regions of the liquid and gas. Please refer to our previous papers[4,17] for algorithmic details.

The underlying computational grid is a dynamic, hierarchical, block structured grid.[42] The Navier-Stokes equations and the deforming boundary equations are discretized using Eulerian finite difference methods. In other words, the liquid/gas interface cuts through the grid; the grid is not body-fitted to the interface. An advantage of our approach is that the grid remains well conditioned regardless of whether the air/water interface undergoes large deformations or perhaps changes in topology. Also, we have developed a very efficient multigrid preconditioned conjugate gradient algorithm[42,43] (MGPCG) for enforcing incompressibility in two phase flows; the MGPCG algorithm is only appropriate for structured (or block-structured) grids. A disadvantage of our approach is that our computational grid will require more memory than an unstructured body-fitted or overlapping grid. A body-fitted grid enables one to exploit large aspect ratio elements around boundaries in order to resolve boundary layers. We feel that the advantages of an Eulerian formulation (being able to use MGPCG, grid regularity throughout the deformation of a bubble/drop) outweigh the disadvantages (requiring more grid points) for simulating skirted bubbles/drops.

A brief outline of the temporal discretization of the two-phase flow equations are as follows:

1. Calculate the time step Δt.
2. Update the position of the interface by discretizing the volume-of-fluid (5) and the level set (6) equations

$$F_t + \boldsymbol{u} \cdot \nabla F = 0, \quad \phi_t + \boldsymbol{u} \cdot \nabla \phi = 0. \tag{10}$$

3. Calculate a provisional velocity field

$$\boldsymbol{u}^* = \boldsymbol{u}^n + \Delta t \left(-(\boldsymbol{u} \cdot \nabla \boldsymbol{u}) + \frac{1}{Re} \frac{1}{\rho} \nabla \cdot (2\mu D) - \frac{1}{We} \kappa \nabla H / \rho + \frac{1}{Fr} \hat{z} \right)^n. \tag{11}$$

4. Projection step

$$\nabla \cdot \frac{\nabla p}{\rho} = \frac{1}{\Delta t} \nabla \cdot \boldsymbol{u}^*, \tag{12}$$

$$\boldsymbol{u}^{n+1} = \boldsymbol{u}^* - \Delta t \frac{\nabla p}{\rho}. \tag{13}$$

Remarks:

- At "outflow" boundaries, the pressure p is specified to have the hydrostatic pressure,

$$p = -\frac{1}{Fr} \rho_S z. \tag{14}$$

- At "inflow" boundaries, the pressure p has the following boundary condition:

$$\frac{1}{\rho} \frac{\partial p}{\partial n} = \frac{u_n^* - u_n}{\Delta t}, \tag{15}$$

where n is the direction normal to the wall and u_n is the normal component of the velocity prescribed at the inflow wall.

III. RESEARCH TARGETS AND COMPUTATIONAL CONDITIONS

A. Research targets

Shapes and terminal velocities of single bubbles or drops moving freely in viscous liquids were organized by Grace *et al.*[44] and Bhaga and Weber[36] based on Re, Eo ($=|\rho_S - \rho_B|gd^2/\sigma$) and M ($= |\rho_S - \rho_B|g\mu_S^4/(\rho_S^2\sigma^3)$). According to the correlation diagram presented by Bhaga and Weber,[36] the condition of "skirted bubbles" lies in limited regions, and these regions are further categorized into two types of skirted bubble motion: (1) the skirted bubble with a smooth, steady skirt and (2) the skirted bubble with a wavy, unsteady skirt. Instead of classifying skirted bubbles/drops by the characteristics of the skirt, Bhaga[1] classified skirted bubbles/drops by the characteristics of the main body of the bubble/drop: (1) the oblate ellipsoidal skirted bubble or drop, (2) the prolate ellipsoidal skirted bubble or drop, and (3) the spherical skirted bubble or drop. In this paper, we shall restrict our study to the motion of a single skirted bubble/drops with the physical properties corresponding to a skirted bubble with a smooth, steady skirt as classified by Bhaga and Weber.[36] Specifically, the condition of $Re = 18.3$, $Eo = 339$, and $M = 43.1$ is used in our computations. Keeping these values for Re, Eo, and M fixed, we shall vary the density ratio λ and the viscosity ratio η.

B. Theory of skirt thickness

In 1969, Guthrie and Bradshaw[11] developed a theory on predicting the skirt thickness of bubbles by considering a simplified flow in which the skirt is perpendicular to the base of a bubble and the skirt forms a two-dimensional thin slab with uniform thickness. Guthrie and Bradshaw[11] derived the following theoretical skirt thickness (δ_{th}):

$$\delta_{th} = \sqrt{\frac{\alpha\mu_B U_S}{\rho_S g}}. \tag{16}$$

In Eq. (16), U_S denotes the outer surface velocity of the suspending fluid down the skirt and is approximated by $U_S \approx U_T$. $\alpha = 12$ for the case in which the gas velocity distribution within the skirt is characterized by a symmetrical profile and $\alpha = 6$ for the case in which an asymmetrical gas velocity profile within the skirt is formed. In other words, $\alpha = 12$ is applicable when a recirculating wake exists in the region surrounded by the skirt and U_W (the velocity of the suspending fluid down the inside surface of the skirt) can be approximated by $U_W \approx U_S$. $\alpha = 6$ applies if the wake enclosed by the skirt is stagnant.

Following the work of Guthrie and Bradshaw,[11] Wairegi[7] presented a general expression for skirt thickness valid for both bubbles and drops. In considering the case when $U_W \ll U_S$, Wairegi[7] obtained the following equation:

$$\delta_{th} = \sqrt{\frac{6\mu_B U_T}{(\rho_S - \rho_B)g}}. \tag{17}$$

The work of Wairegi[7] was further refined by Bhaga[1] who introduced a shape dependent thickness coefficient S and a correction factor C_f for deviation from potential flow in order to derive the following model for skirt thickness:

$$\delta_{th} = S\sqrt{\frac{\alpha C_f \mu_B U_T}{(\rho_S - \rho_B)g}}. \tag{18}$$

S is a function of the main body shape of a bubble/drop and S varies based on whether a bubble/drop has an oblate ellipsoidal, prolate ellipsoidal, or spherical shape. The deviation parameter from potential flow C_f satisfies $C_f \approx 1$ for high Re conditions and $C_f < 1$ for low Re conditions.

Equation (18) can be rewritten as follows:

$$\delta_{th} = A\sqrt{\frac{\mu_B U_T}{(\rho_S - \rho_B)g}}, \tag{19}$$

where A is $\sqrt{6S^2C_f}$. The value of A will be almost identical irrespective of bubbles and drops if one fixes at the same time the values of Re, Eo, M, and η. After one nondimensionalizes Eq. (19) with respect to d, one finds

$$\delta_{th}^* = \frac{\delta_{th}}{d} = A\sqrt{\frac{\mu_B U_T}{d^2(\rho_S - \rho_B)g}} = A\sqrt{\frac{Fr \cdot \eta}{Re(1-\lambda)}} = A\sqrt{\frac{\eta Re M^{1/2}}{Eo^{3/2}}}. \tag{20}$$

Equation (20) implies that δ_{th}^* has the same value regardless of bubbles and drops once the parameters Re, Eo $(=We(1-\lambda)/Fr)$, M $(=We^2Eo/Re^4)$, η are fixed to the same value. We shall find below, through numerical simulation, that Eq. (20) must be modified in order to take into account a varying λ while at the same time fixing the remainder four dimensionless quantities η, Re, M, and Eo. In other words, we have discovered that fixing the density jump, $\Delta\rho = \rho_S - \rho_B$, η, Re, M, and Eo, while at the same time only varying ρ_B/ρ_S, causes a variation in the skirt thickness.

C. Computational grid

The computational grid established for numerically solving the buoyancy-driven motion of bubbles and drops is shown in Figure 1. The computational grid consists of an axisymmetric cylindrical computational domain with dimensions of 2.5 (r-direction) $\times$ 5.0 (z-direction) in size with respect to the dimensionless diameter D $(= 1.0)$. Initially, a spherical bubble or drop is artificially imposed at the center of the computational domain. The boundary conditions for our numerical simulations are as follows:

- **center,** $r = 0$: Reflecting boundary conditions are used for the pressure p and the vertical velocity w. The velocity u in the r direction is zero at $r = 0$.
- **right wall,** $r = 2.5$: We treat the right wall as an "outflow" wall in which the velocity on the boundary is copied from the velocity just inside the right wall. The pressure on the right wall is specified to be $p = -\frac{1}{Fr}\rho_S z$ (14).

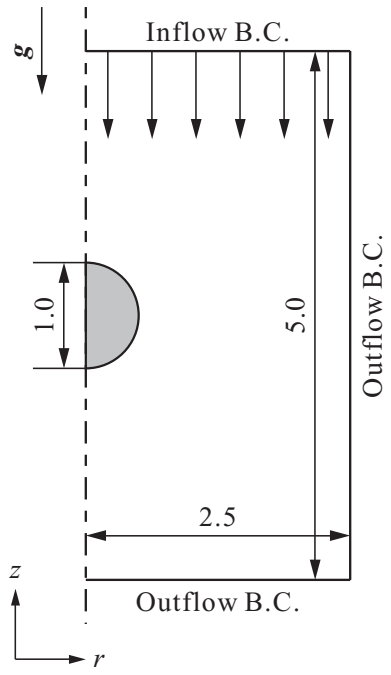

FIG. 1. Computational system.

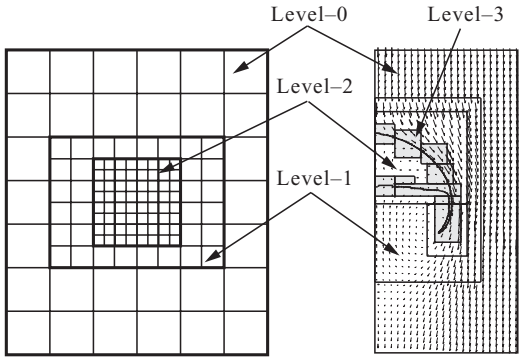

FIG. 2. Grid structure using the adaptive mesh refinement (AMR) system.

- **top wall,** $z = 5$**:** We treat the top wall as an "inflow" wall in which the radial velocity is $u = 0$ and the dimensionless vertical velocity is $w_{wall} = -1.0$. The pressure on the top wall satisfies a Neumann boundary condition (15): $\frac{1}{\rho_S}\frac{\partial p}{\partial z} = \frac{w^* - w_{wall}}{\Delta t}$.
- **bottom wall,** $z = 0$**:** We treat the bottom wall as an "outflow" wall in which the velocity on the boundary is copied from the velocity just inside the bottom wall. The pressure on the bottom wall is specified to be $p = 0$ (14).

In order to carry out the computations as efficiently as possible, we represent the computational domain as an adaptive hierarchy of rectangular grids (adaptive mesh refinement (AMR)[42,45]) as opposed to a single, uniform, rectangular grid. Figure 2 shows a schematic drawing of the AMR system. The left panel of Fig. 2 is an example of the hierarchical grid structure and the right panel of Fig. 2 illustrates a computational example for a rising skirted drop. The mesh hierarchy is composed of multiple levels of refinement ranging from coarsest ($\ell = 0$, labeled as "Level-0") to finest ($\ell = \ell_{max}$, labeled as "Level-6"). In Fig. 2, four levels (Level-0, Level-1, Level-2, and Level-3) are illustrated as an example; the refinement ratio between the levels is 2. Since the refinement ratio is 2, we have $\Delta x^{\ell+1} = \Delta x^{\ell}/2$ (Δx: the size of a side of a single computational cell). Adaptive mesh refinement enables one to dynamically cluster grid points around portions of the computational domain where the gradient is large (i.e., where the deforming bubble/drop interface is).

D. Validation of numerical method for bubbles and drops

We validate our numerical method in three different ways:

(1) We compare simulated results of a buoyantly rising bubble/drop with previously reported experimental observations.
(2) We check the sensitivity of numerical results to the type of "sharp interface" formulation used.
(3) We compare simulated results on a coarse mesh with corresponding results on a fine mesh.

We shall discuss items (1) and (2) in this section and item (3) will be discussed with physical insight throughout Sec. IV.

1. Comparison of numerical results with benchmark experimental results for bubble/drop rise motion

We compare numerical predictions using our adaptive mesh refinement-coupled level-set and volume-of-fluid ("AMR-CLSVOF') algorithm with previous experimental results, for a variety of physical properties, presented by Bhaga and Weber.[36] Specific physical properties of 10 conditions and a comparison of the numerical prediction of *Re* with the corresponding experimental observation are tabulated in Table II. In Table II, Re_{exp} is the experimental *Re* reported by Bhaga and Weber[36] and Re_{cal} corresponds to the computational *Re* predicted by our computations (AMR-CLSVOF). For the results in Table II, the finest level mesh size was $\Delta x^{fine} = 0.0098D$ ($D = 1.0$), the density ratio was

TABLE II. Comparison of our computational results with previous experimental results by Bhaga and Weber.[36]

Condition	Eo	M	Re_{exp}	Re_{cal}	Re_{cal}/Re_{exp}
1	8.67	711	0.078	0.078	1.00
2	17.7	711	0.232	0.232	1.00
3	243	266	7.77	7.80	1.00
4	116	848	2.47	2.47	1.00
5	116	266	3.57	3.57	1.00
6	116	41.1	7.16	7.16	1.00
7	116	5.51	13.3	13.3	1.00
8	116	1.31	20.4	20.4	1.00
9	116	0.103	42.2	41.2	0.98
10	115	4.63×10^{-3}	94.0	94.8	1.01

$\lambda = 1.0 \times 10^{-3}$ and the viscosity ratio was $\eta = 1.0 \times 10^{-4}$. Figure 3 shows a comparison between the experimentally observed bubble shapes (left) and the numerical prediction (right). The results reported in Table II and Fig. 3 show good agreement between numerical results and experiments.

2. Sensitivity of the numerical results to the type of "sharp interface formulation" used

We compared the following two sharp interface methods: (i) the sharp interface method (SIM) described in Ref. 4 in which an additional liquid velocity variable is maintained throughout the simulation, and (ii) the sharp interface method (SIM) described in Ref. 4 in which an additional liquid velocity variable is not maintained (only the total/combined velocity field is stored and maintained). SIM (ii) is also known as the ghost fluid method.[16] Both "SIM (i)" and "SIM (ii)" are consistent discretizations for two phase flows. For many test problems, we found "SIM (i)" to be more accurate than "SIM (ii)" in the limiting case of zero gas density and zero gas viscosity.[4,46] On the other hand, "SIM (i)" has lower accuracy than "SIM (ii)" for moderate density/viscosity ratio problems.[47] In our study of skirted bubble/drop dynamics, we choose to use the formulation "SIM (ii)" for both the skirted drop (moderate density ratio) problems and for the skirted bubble (large density ratio) problems. We have found that, for skirted bubble calculations, there was no significant advantage in using "SIM (i)" over "SIM (ii)." Figure 4 shows a comparison between "SIM (i)" and "SIM (ii)" for a bubble rising with the properties $Re = 18.3$, $Eo = 339$, $M = 43.1$, $\lambda = 1.4 \times 10^{-3}$, and $\eta = 1.0 \times 10^{-3}$. The left panel shows a comparison of the bubble shape and the right panel shows a comparison of the computed Re number versus dimensionless time. This comparison was carried out with a grid size of $\Delta x^{fine} = 1/512$. We find that computational results based on "SIM (i)" and "SIM (ii)" agree well with each other.

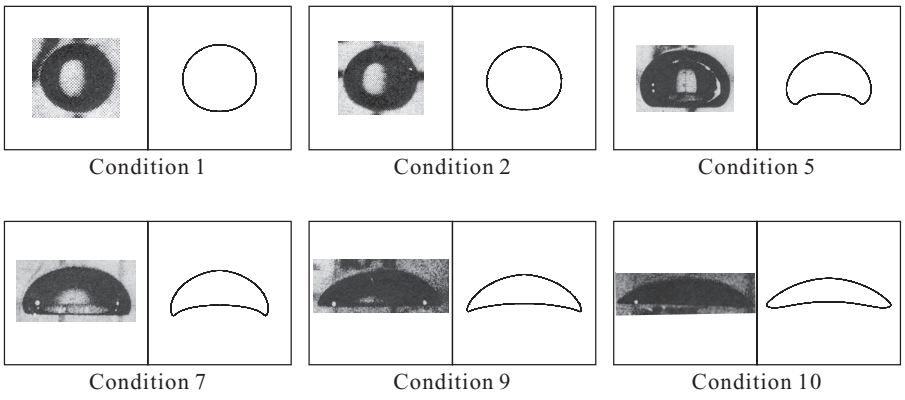

FIG. 3. Comparisons of our computational results with experimental results by Bhaga and Weber.[36]

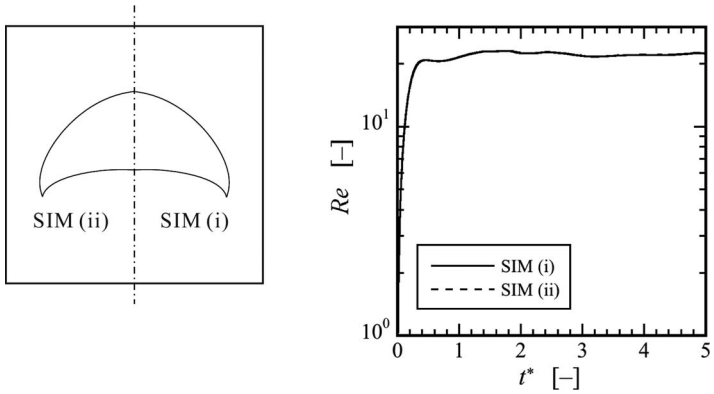

FIG. 4. Comparison of results obtained using "sharp interface method (i)" (additional liquid velocity field is maintained throughout the simulation) and "sharp interface method (ii)" (only the total/combined velocity field is maintained). These are computational results for a bubble with the condition of $Re = 18.3$, $Eo = 339$, $M = 43.1$. (Left) Bubble shape. (Right) The time change in the Re number.

IV. RESULTS AND DISCUSSION

A. Effect of density ratio λ on the skirt thickness

In this section, we consider the sensitivity of skirt thickness with respect to λ. Tables III and IV show the physical conditions used for our computations of skirted bubbles and drops in which we investigate the effect of λ. The physical parameters, except for λ, are fixed to $Re = 18.3$, $Eo = 339$, $M = 43.1$, and $\eta = 1.0 \times 10^{-3}$. The computed bubble shapes corresponding to the physical conditions in Tables III and IV are shown in Figures 5 and 6, respectively.

Some of the conditions in Tables III and IV have an unrealistic density, but the setting of these densities is done in a strategic fashion so that we can deduce more information on the relation between skirt thickness and the density ratio. We define "skirted bubble flow" to be the case when λ is on the order of $0.1 \sim 0.001$; we define "skirted drop flow" to correspond to all other cases of (moderate) λ.

Figure 5 shows computational results corresponding to the 8 conditions tabulated in Table III. In these computations, we set $\Delta x^{fine} = 1/512$ in the vicinity of the deforming interface, and computations were implemented by solving the dimensionless governing equations as described in Sec. II. What we observe from Figure 5, is that the thickness of a trailing skirt from a buoyantly rising drop/bubble is sensitive to λ, even if the density jump ($\Delta\rho$) is fixed. In other words, two bubbles/drops sharing the same $\Delta\rho$ but a different λ can have different skirt thicknesses. This observation is contrary to the prevailing theory described in the study of Bhaga[1] and explained by Eq. (20). We find that δ^*_{th} varies depending on the physical conditions even if the set of parameters Re, Eo, M, η are fixed to the same values. The non-skirted shapes in Figure 5 are spherical-cap type shapes and that one can regard the

TABLE III. Computational conditions for investigating the effect of λ. Other conditions are fixed to $Re = 18.3$, $Eo = 339$, $M = 43.1$, $\eta = 1.0 \times 10^{-3}$.

Case	ρ_S [kg/m^3]	ρ_B [kg/m^3]	$\Delta\rho$ [kg/m^3]	λ [–]
1	1000	990	10	0.990
2	1000	900	100	0.900
3	200	100	100	0.500
4	1000	700	300	0.700
5	301	1	300	0.003
6	1400	800	600	0.571
7	601	1	600	0.002
8	801	1	800	0.001

TABLE IV. Computational conditions for investigating the effect of the density ratio λ and the effect of increasing grid resolution. Conditions other than λ are fixed to $Re = 18.3$, $Eo = 339$, $M = 43.1$, $\eta = 1.0 \times 10^{-3}$.

Case	ρ_S [kg/m^3]	ρ_B [kg/m^3]	$\Delta\rho$ [kg/m^3]	λ [–]
A	1400	700	700	0.500
B	933	233	700	0.250
C	778	78	700	0.100
D	701	1	700	0.001

sharp edge at the bottom of the bubble as a very short skirt or as at least the basing point of skirt generation. The computational results for the non-skirted shapes can be interpreted as predicting a skirt that is one-grid cell thick. We note that if we increase the grid resolution from $\Delta x^{fine} = 1/512$ to $\Delta x^{fine} = 1/1024$, we do capture the thin skirt corresponding to case B in Figure 6.

We note that for the low resolution case of drop B (the effective fine grid resolution is $\Delta x^{fine} = 1/512$), short skirts are generated, but the skirt was continuously torn from the sharp edge. The progression for case B, from "not skirted" on the low resolution AMR grid, to "skirted" on the high resolution AMR grid is expected. The juxtaposition of the results for case A (parameters expected to reproduce a relatively thick skirted drop) with case B (parameters expected to reproduce a relatively thin skirted drop) shows our numerical method enables one to reproduce skirted bubbles and drops only when we use an effective fine grid resolution that is about an order of magnitude smaller than the skirt thickness.

The non-dimensional experimental skirt thickness δ^*_{exp} for bubbles measured by Guthrie and Bradshaw,[11] under similar conditions as our case D (their conditions were $Re = 23.2$, $Eo = 423$, $M = 69.8$, $\lambda = 9.2 \times 10^{-4}$, and $\eta = 1.4 \times 10^{-5}$), yields $\delta^*_{exp} = 5.8 \times 10^{-4}$ to 1.2×10^{-3}. Our finest grid resolution result, $\Delta x^{fine} = 1/1024$ ($\approx 9.8 \times 10^{-4}$), is almost on the same order as 1.0×10^{-3}. We expect that a grid size with $\Delta x^{fine} \approx 1.0 \times 10^{-4}$ will be required for numerically capturing the very thin skirt. At the same time, regarding the skirt thickness for the drops in Fig. 6, δ^*_{exp} for the experimental conditions of $Re = 8.0 \sim 16.3$, $Eo = 150 \sim 185$, $M = 8.6 \sim 85.4$, $\lambda = 0.62 \sim 0.81$, and $\eta = 8.0 \times 10^{-3} \sim 5.3 \times 10^{-2}$, is in the range of $\delta^*_{exp} = 1.6 \times 10^{-2}$ to 4.6×10^{-2} (Bhaga[1]). Taking these values of δ^*_{exp} for drops into consideration, our computed skirted drops, cases 1–4 and 6 in Table III and case A in Table IV, successfully reproduced experimental results using a grid size of $\Delta x^{fine} = 1/512$ ($\approx 2.0 \times 10^{-3}$). If the dimensionless experimental skirt thickness is on the order of 2×10^{-2}, then a numerical resolution of 2.0×10^{-3} is sufficient to resolve the skirts of a rising drop.

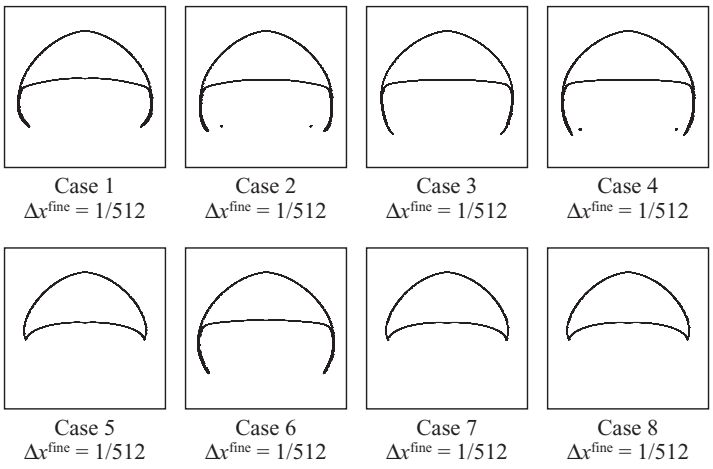

FIG. 5. Computational results depending on λ. Physical conditions are $Re = 18.3$, $Eo = 339$, $M = 43.1$, $\eta = 1.0 \times 10^{-3}$. For cases 1-8, λ is 0.990, 0.9, 0.5, 0.7, 0.003, 0.571, 0.002, and 0.001, respectively.

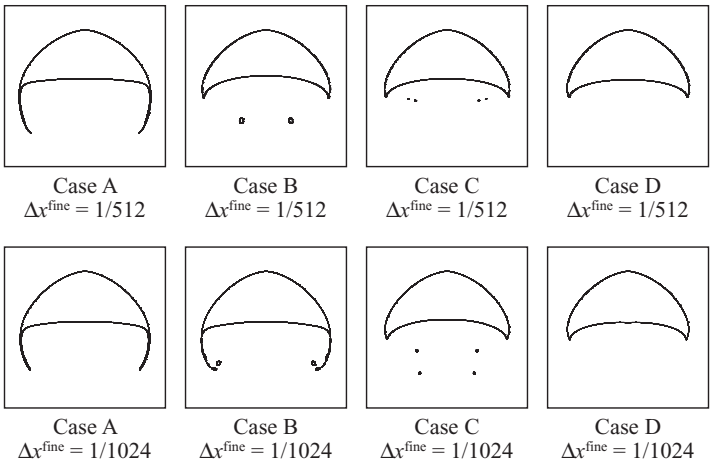

FIG. 6. Computational results depending on λ and the grid resolution. Physical conditions are $Re = 18.3$, $Eo = 339$, $M = 43.1$, $\eta = 1.0 \times 10^{-3}$. From left to right, λ is 0.5, 0.25, 0.1, and 0.001.

In Figure 7, we investigate the detailed flow fields for cases A (density ratio $\lambda = 0.5$) and D (density ratio $\lambda = 0.001$) for the grid resolution of $\Delta x^{fine} = 1/512$ (dimensionless units). In this figure, we show a progression of the flow field from the initial formation of a skirt to the computed steady profile. The flow field is illustrated in a frame of reference moving vertically with dimensionless unit speed. From this figure, we observe that even in the beginning stages of skirt formation, the transient skirt for case A is thicker than for case D. As the flow develops, both cases illustrate a progressive thinning of the skirt towards a steady shape. From looking at the instantaneous streamlines for Figure 7, we see that the skirted case A develops just one "circulation lobe" about the rim of the drop whereas the non-skirted case D develops two "circulation lobes" about the rim of the bubble. Finally, we also illustrate the dimensionless "reduced pressure" field in Figure 7. The reduced pressure is defined as $p + \frac{1}{Fr}\rho z$. The reduced pressure in the bubble/drop varies only slightly in space with the largest values occurring at the rim of the bubble/drop where the curvature is largest.

B. Effect of viscosity ratio on skirt thickness

In this section, we explore the relation between the viscosity ratio η and the skirt thickness. Whereas λ is only implicitly taken into account in the expression for δ^*_{th} (20) (λ is in the expression for Eo), η is explicitly found in Eq. (20). We use cases A ($\lambda = 0.5$) and D ($\lambda = 0.001$) with a grid size of $\Delta x^{fine} = 1/512$ as a starting point for studying the effects of η. These two cases were selected because of the large difference in λ between them.

The computational conditions for investigating the effect of η are tabulated in Table V. Figure 8 shows the computational results, as a function of η, corresponding to the computational conditions in Table V. The physical parameters, other than η and λ, are set to $Re = 18.3$, $Eo = 339$, $M = 43.1$.

TABLE V. Computational conditions for investigating the effect of η. Other conditions are fixed to $Re = 18.3$, $Eo = 339$, $M = 43.1$.

Case	ρ_S [kg/m^3]	ρ_B [kg/m^3]	$\Delta\rho$ [kg/m^3]	λ [–]	η [–]
A-1	1400	700	700	0.500	1.00
A-2	1400	700	700	0.500	0.10
A-3	1400	700	700	0.500	1.0×10^{-3}
A-4	1400	700	700	0.500	1.0×10^{-5}
D-1	701	1	700	0.001	1.00
D-2	701	1	700	0.001	0.10
D-3	701	1	700	0.001	1.0×10^{-3}
D-4	701	1	700	0.001	1.0×10^{-5}

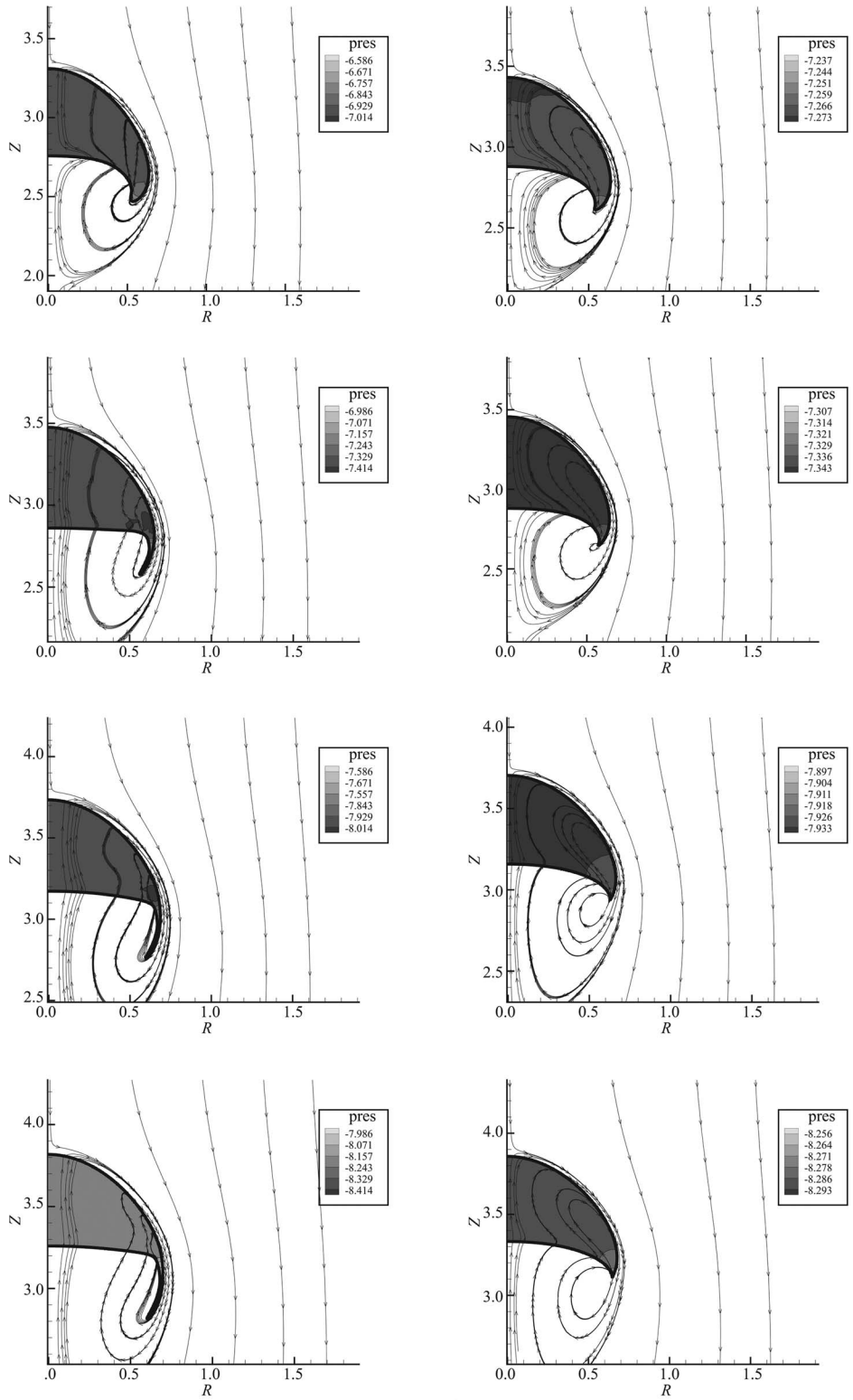

FIG. 7. Flow detail for cases A (left, $\lambda = 0.5$) and D (right, $\lambda = 0.001$). Physical conditions are $Re = 18.3$, $Eo = 339$, $M = 43.1$, $\eta = 1.0 \times 10^{-3}$. Grid size on finest level is $\Delta x^{fine} = 1/512$. The dimensionless times for the case A frames are (from top to bottom) 2.0, 3.0, 4.6, and 5.1. For case B, the times are 1.7, 1.9, 3.8, and 5.1. The darker shaded region within each bubble represents a low reduced pressure region and the lighter shaded region at the bubble rim represents a slightly higher reduced pressure region. Reduced pressure is $p + \frac{1}{Fr}\rho z$.

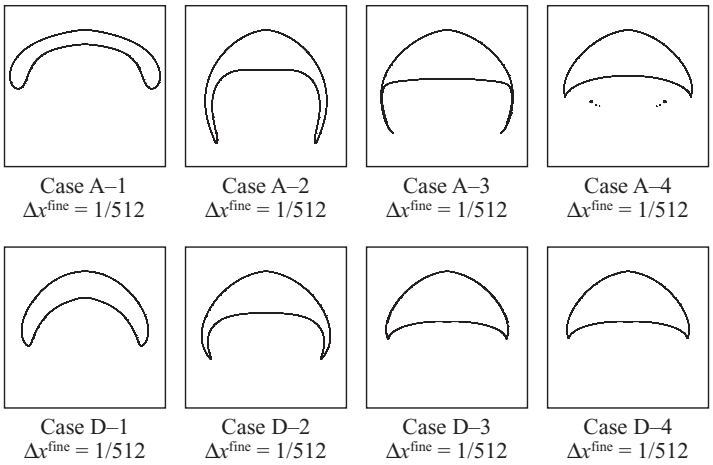

FIG. 8. Computational results depending on η. Physical conditions are $Re = 18.3$, $Eo = 339$, $M = 43.1$. (Top row) $\lambda = 0.5$. (Bottom row) $\lambda = 0.001$. From left to right, $\eta = 1.0$, $\eta = 0.1$, $\eta = 1.0 \times 10^{-3}$, and $\eta = 1.0 \times 10^{-5}$. The grid size with $\Delta x^{fine} = 1/512$ was used.

As seen from Fig. 8, and also predicted by Eq. (20), the skirt thickness decreases with decreasing η. When $\eta = 1.0 \times 10^{-5}$ (cases A-4 and D-4), the skirt is too thin for us to resolve with a grid size of $\Delta x^{fine} = 1/512$. In Table VI, we compare the computed dimensionless skirt thickness, as a function of η ($\eta = 0.01, 0.025, 0.05, 0.075, 0.1$), with the square root dependence on η predicted by Eq. (20). We derived the skirt thickness from our simulations by measuring the skirt thickness at a vertical (z coordinate) position corresponding to the largest extent of the skirt in the radial r direction.

We note that in the extreme case of large η, $\eta = 1.0$, the bubble/drop shifts from the skirted regime. This phenomena falls outside the region of validity of the theory developed by Bhaga and Weber[36] because Re, Eo, and M lie in the "skirted bubble regime" but our computed shape is not a skirted bubble/drop. This phenomena would be difficult to reproduce experimentally, as we have used extreme values for the "physical properties." A numerical algorithm has the "enabling" capability to predict flows of fictitious "exotic" materials. We note that we report in Ref. 47 the results on the sensitivity of bubble/drop shape due to varying viscosity and density ratio. The work here is unique from Ref. 47 in that we consider the effect on skirts of the density and viscosity ratio. Since $\eta = 1$ does not correspond to a skirted bubble/drop, we shall address the cases when $\eta < 1$ when analyzing the effect of η on the skirt thickness.

Figure 8 shows that the effect of η is much more prominent on the skirt thickness than the effect of λ. Figure 8 also illustrates that there is a slight effect on the skirt thickness by varying λ. Skirted bubbles have thinner skirts than skirted drops, all other parameters being equal (Re, Eo, M, $\Delta\rho$, η). There is a slight synergistic effect in varying both λ and η. The rate of increase of the skirt thickness with increasing η is higher for the skirted drops than the skirted bubbles.

In Figure 9, we investigate the detailed flow fields for cases A-1 (viscosity ratio $\eta = 1$) and A-2 (viscosity ratio $\eta = 0.1$) for the grid resolution of $\Delta x^{fine} = 1/512$. In this figure, we show a

TABLE VI. Comparison of the computed dimensionless skirt thickness with the square root dependence on skirt thickness predicted by (20). All dimensionless quantities, other than η, are fixed to $Re = 18.3$, $Eo = 339$, $M = 43.1$, and $\lambda = 0.5$. $\Delta x^{fine} = 1/512$.

η	Computed skirt thickness	Predicted $\sqrt{\eta}$ dependence
0.01	0.035	0.028
0.025	0.052	0.044
0.05	0.068	0.063
0.075	0.079	0.077
0.1	0.089	0.089

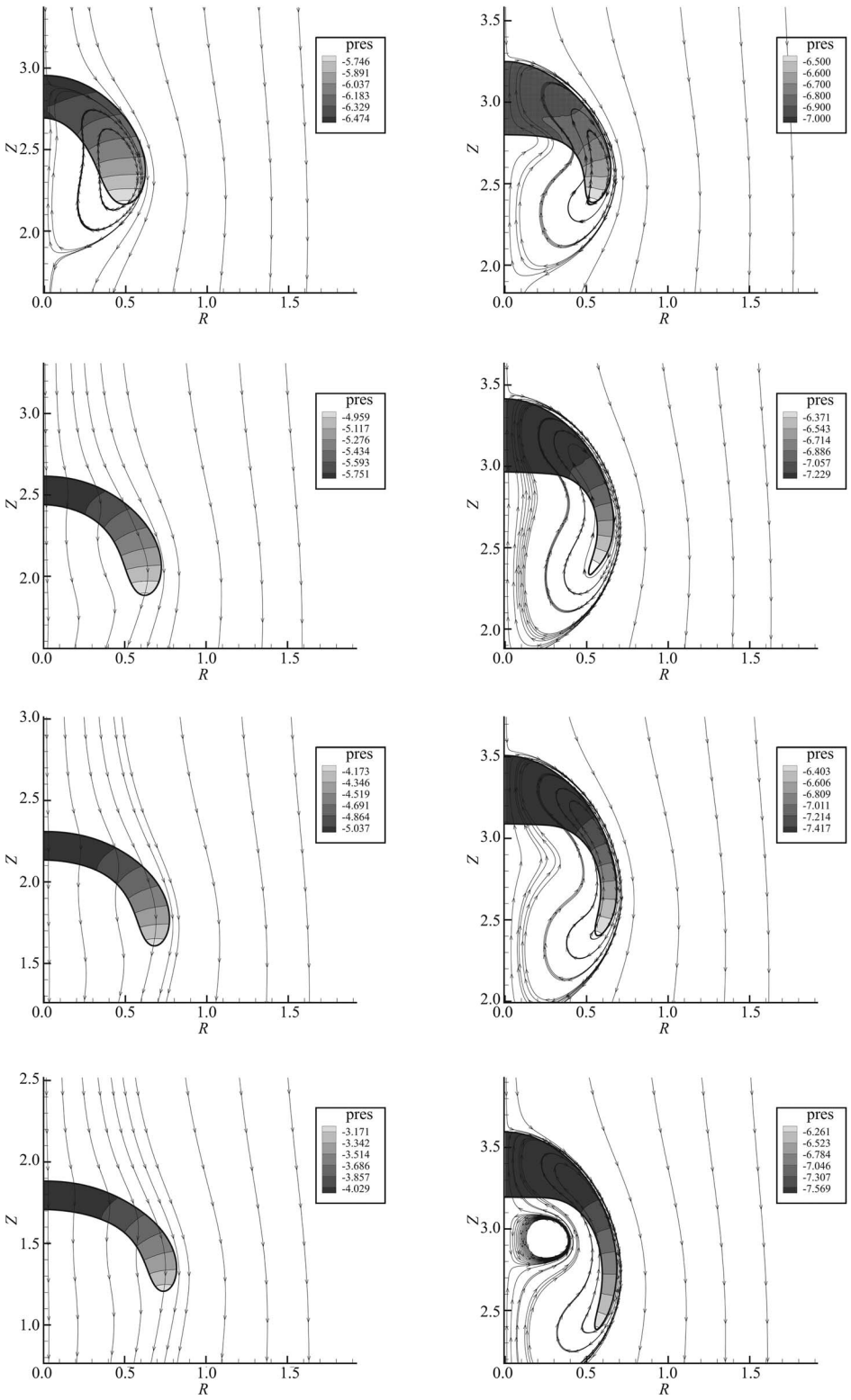

FIG. 9. Flow detail for cases A-1 (Left, $\eta = 1.0$) and A-2 (Right, $\eta = 0.1$). Physical conditions are $Re = 18.3$, $Eo = 339$, $M = 43.1$, $\lambda = 1/2$. Grid size on finest level is $\Delta x^{fine} = 1/512$. The dimensionless times for the case A-1 and A-2 frames are (from top to bottom) 2.5, 4.6, 5.8, and 7.4. The darker shaded region within each bubble represents a low reduced pressure region and the lighter shaded region at the bubble rim represents a slightly higher reduced pressure region. Reduced pressure is $p + \frac{1}{Fr}\rho z$.

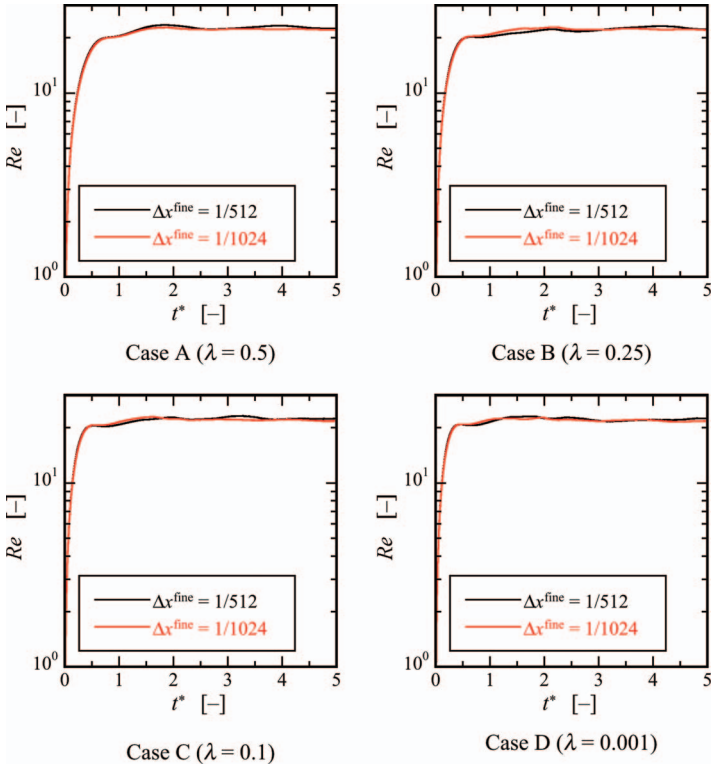

FIG. 10. The time variation in Re depending on λ. Physical conditions are $Re = 18.3$, $Eo = 339$, $M = 43.1$, $\eta = 1.0 \times 10^{-3}$.

progression of the flow field, contrasting the two different cases: (1) A-1 ($\eta = 1$) does not develop a skirt, and (2) A-2 ($\eta = 0.1$) does develop a skirt. The flow field is illustrated in a frame of reference moving vertically with dimensionless unit speed. We also illustrate the dimensionless "reduced pressure" field in Figure 9. The reduced pressure is defined as $p + \frac{1}{Fr}\rho z$. The reduced pressure in the bubble/drop varies only slightly in space with the largest values occurring at the rim of the bubble/drop where the curvature is largest.

C. The effect of skirt thickness on the rise velocity

In Figure 10, the velocity as a function of dimensionless time (Re versus t^*) is reported for the skirted bubbles/drops shown in Fig. 6 (physical properties are reported in Table IV). We first observe from Figs. 6 and 10 that, as far as capturing the correct rise speed is concerned, an effective fine grid resolution of $\Delta x^{fine} = 1/512$ is sufficient to capture the correct rise speed. The rise speed for the low resolution simulations (effective fine grid resolution is $\Delta x^{fine} = 1/512$) matches closely the rise speed for the high resolution simulations (effective fine grid resolution is $\Delta x^{fine} = 1/1024$).

We also observe from case (B) of Figs. 6 and 10 that the presence of a skirt does not effect the drop rise speed. The high resolution simulation, $\Delta x^{fine} = 1/1024$, and the low resolution simulation, $\Delta x^{fine} = 1/512$, both predict the same rise speed, but the high resolution case has a trailing skirt.

V. CONCLUSIONS

The buoyancy-driven motion of a single skirted bubble or drop rising through viscous liquids was simulated using a 3D axisymmetric numerical algorithm in which the CLSVOF method was used to approximate the deforming boundary and a sharp interface technique was employed for treating the interface jump conditions. In particular, we investigated the sensitivity of skirted bubble/drop motion

due to a varying density ratio λ and/or viscosity ratio η. The following is a list of our findings:

1. The previous theory (Eq. (20)) does not take into account a varying λ (keeping Re, η, M, and Eo fixed). We have found that the skirt thickness increases with increasing λ keeping all other dimensionless quantities fixed.
2. There is a synergistic effect in varying both λ and η. In other words, the sensitivity of skirt thickness due to varying η, while keeping Re, M, and E_o fixed, is different when λ corresponds to a "bubble" ($\lambda = 0.001$) versus when λ corresponds to a "drop" ($\lambda = 0.5$).
3. Our computational results indicate that the presence of "thin" skirts have little effect on the rise velocity.

In this paper, we numerically studied the sensitivity of skirt thickness due to varying physical properties of the suspending fluid and bubble (drop). In future work, fully 3D effects and bubble compressibility can be investigated. For the case of skirted bubbles with λ on the order of 1/1000 and η on the order of 1/100, our present numerical method requires a prohibitive amount of grid resolution. We have very recently started investigating moment-of-fluid methods for simulating multiphase flow problems with thin structures.[48] The results in Ref. 48 are promising. We are now developing an even further improved moment-of-fluid method, which can "capture" thin structures which would enable us to meet ever more stringent challenges in studying singly rising skirted bubbles and drops or studying the interaction of many bubbles/drops.

[1] D. Bhaga, "Bubbles in viscous liquids: Shapes, wakes and velocities," Ph.D. dissertation (McGill University, 1976).
[2] A. Gupta and R. Kumar, "Lattice Boltzmann simulation to study multiple bubble dynamics," Int. J. Heat Mass Transfer **51**, 5192–5203 (2008).
[3] M. Ohta, T. Imura, Y. Yoshida, and M. Sussman, "A computational study of the effect of initial bubble conditions on the motion of a gas bubble rising in viscous liquids," Int. J. Multiphase Flow **31**, 223–237 (2005).
[4] M. Sussman, K. M. Smith, M. Y. Hussaini, M. Ohta, and R. Zhi-Wei, "A sharp interface method for incompressible two-phase flows," J. Comp. Phys. **221**(2), 469–505 (2007).
[5] J. J. Thomson and H. F. Newall, "On the formation of vortex rings by drops falling into liquids, and some allied phenomena," Proc. R. Soc. London **39**, 417–436 (1885).
[6] P. D. Shoemaker and L. E. Marc De Chazal, "Dimpled and skirted liquid drops moving through viscous liquid media," Chem. Eng. Sci. **24**, 795–797 (1969).
[7] T. Wairegi, "The mechanics of large bubbles and drops moving through extended liquid media," Ph.D. dissertation (McGill University, 1974).
[8] T. Wairegi and J. R. Grace, "The behaviour of large drops in immiscible liquids," Int. J. Multiphase Flow **3**, 67–77 (1976).
[9] H. Angelino, "Hydrodynamique des grosses bulles dans les liquides visqueux," Chem. Eng. Sci. **21**, 541–550 (1966).
[10] W. G. Davenport, F. D. Richardson, and A. V. Bradshaw, "Spherical cap bubbles in low density liquids," Chem. Eng. Sci. **22**, 1221–1235 (1967).
[11] R. I. L. Guthrie and A. V. Bradshaw, "The stability of gas envelopes trailed behind large spherical cap bubbles rising through viscous liquids," Chem. Eng. Sci. **24**, 913–917 (1969).
[12] R. I. L. Guthrie and A. V. Bradshaw, "Spherical capped gas bubbles rising in aqueous media," Chem. Eng. Sci. **28**, 191–203 (1973).
[13] P. H. Calderbank, D. S. L. Johnson, and J. Loudon, "Mechanics and mass transfer of single bubbles in free rise through some newtonian and non-newtonian liquids," Chem. Eng. Sci. **25**, 235–256 (1970).
[14] P. P. Wegener, R. E. Sundell, and J.-Y. Parlange, "Spherical cap bubbles rising in liquids," Z. Flugwiss. **19**, 347–352 (1971).
[15] J. G. Hnat and J. D. Buckmaster, "Spherical cap bubbles and skirt formation," Phys. Fluids **19**, 182–194 (1976).
[16] M. Kang, R. Fedkiw, and X.-D. Liu, "A boundary condition capturing method for multiphase incompressible flow," J. Sci. Comput. **15**, 323–360 (2000).
[17] P. A. Stewart, N. Lay, M. Sussman, and M. Ohta, "An improved sharp interface method for viscoelastic and viscous two-phase flows," J. Sci. Comput. **35**(1), 43–61 (2008).
[18] S. O. Unverdi and G. Tryggvason, "A front-tracking method for viscous, incompressible, multi-fluid flows," J. Comput. Phys. **100**, 25–37 (1992).
[19] M. Sussman and P. Smereka, "Axisymmetric free boundary problems," J. Fluid Mech. **341**, 269–294 (1997).
[20] M. Ohta and M. Suzuki, "Numerical analysis of dispersed drop behavior in the pulsed sieve-plate extraction column," Int. Commun. Heat Mass Transfer **25**, 521–530 (1998).
[21] M. Ohta, S. Haranaka, Y. Yoshida, and M. Sussman, "Three dimensional simulation of the motion of a gas bubble rising in viscous liquid," J. Chem. Eng. Jpn. **37**(8), 968–975 (2003).
[22] T. Inamuro, T. Ogata, and F. Ogino, "Numerical simulation of bubble flows by the lattice Boltzmann method," FGCS, Future Gener. Comput. Syst. **20**, 959–964 (2004).
[23] M. van Sint Annaland, N. G. Deen, and J. A. M. Kuipers, "Numerical simulation of gas bubbles behaviour using a three-dimensional volume of fluid method," Chem. Eng. Sci. **60**, 2999–3011 (2005).
[24] M. van Sint Annaland, W. Dijkhuizen, N. G. Deen, and J. A. M. Kuipers, "Numerical simulation of behavior of gas bubbles using a 3-d front-tracking method," AIChE J. **52**, 99–110 (2006).

[25] T. Bonometti and J. Magnaudet, "An interface-capturing method for incompressible two-phase flows. Validation and application to bubble dynamics," Int. J. Multiphase Flow **33**, 109–133 (2007).
[26] J. Hua and J. Lou, "Numerical simulation of bubble rising in viscous liquid," J. Comput. Phys. **222**, 769–795 (2007).
[27] J. Hua, J. F. Stene, and P. Lin, "Numerical simulation of 3d bubbles rising in viscous liquids using a front tracking method," J. Comput. Phys. **227**, 3358–3382 (2008).
[28] Z. Yu and L.-S. Fan, "Direct simulation of the buoyant rise of bubbles in infinite liquid using level set method," Can. J. Chem. Eng. **86**, 267–275 (2008).
[29] Z. Yu and L.-S. Fan, "An interaction potential based lattice Boltzmann method with adaptive mesh refinement (amr) for two-phase flow simulation," J. Comput. Phys. **228**, 6456–6478 (2009).
[30] Z. Wang, J. Yang, B. Koo, and F. Stern, "A coupled level set and volume-of-fluid method for sharp interface simulation of plunging breaking waves," Int. J. Multiphase Flow **35**, 227–246 (2009).
[31] S. Hysing, S. Turek, D. Kuzmin, N. Parolini, S. Ganesan E. Burman, and L. Tobiska, "Quantitative benchmark computations of two-dimensional bubble dynamics," Int. J. Numer. Methods Fluids **60**, 1259–1288 (2009).
[32] L. Amaya-Bower and T. Lee, "Single bubble rising dynamics for moderate Reynolds number using lattice Boltzmann method," Comput. Fluids **39**, 1191–1207 (2010).
[33] H. Farhat, W. Choi, and J. S. Lee, "Migrating multi-block lattice Boltzmann model for immiscible mixtures: 3d algorithm development and validation," Comput. Fluids **39**, 1284–1295 (2010).
[34] G. Pianet, S. Vincent, J. Leboi, J. P. Caltagirone, and M. Anderhuber, "Simulating compressible gas bubbles with a smooth volume tracking 1-fluid method," Int. J. Multiphase Flow **36**, 273–283 (2010).
[35] R. N. Krishnan, S. Vivek, D. Chatterjee, and S. K. Das, "Performance of numerical schemes in the simulation of two-phase free flows and wall bounded mini channel flows," Chem. Eng. Sci. **65**, 5117–5136 (2010).
[36] D. Bhaga and M. E. Weber, "Bubbles in viscous liquids: Shapes, wakes and velocities," J. Fluid Mech. **105**, 61–85 (1981).
[37] Y. C. Chang, T. Y. Hou, B. Merriman, and S. Osher, "Eulerian capturing methods based on a level set formulation for incompressible fluid interfaces," J. Comput. Phys. **124**, 449–464 (1996).
[38] M. Raessi and H. Pitsch, "Consistent mass and momentum transport for simulating incompressible interfacial flows with large density ratios using the level set method," Comput. Fluids **63**, 70–81 (2012).
[39] M. Sussman and E. G. Puckett, "A coupled level set and volume of fluid method for computing 3D and axisymmetric incompressible two-phase flows," J. Comp. Phys. **162**, 301–337 (2000).
[40] M. Sussman, "A second order coupled levelset and volume of fluid method for computing growth and collapse of vapor bubbles," J. Comput. Phys. **187**, 110–136 (2003).
[41] M. Sussman, P. Smereka, and S. J. Osher, "A level set approach for computing solutions to incompressible two-phase flow," J. Comput. Phys. **114**, 146–159 (1994).
[42] M. Sussman, "A parallelized, adaptive algorithm for multiphase flows in general geometries," Comput. Struct. **83**, 435–444 (2005).
[43] O. Tatebe, "The multigrid preconditioned conjugate gradient method," in *Proceedings of the 6th Copper Mountain Conference on Multigrid Methods, NASA conference publication 3224, part 2, Copper Mountain, CO, 4–9 April 1993*, edited by N. D. Melson, T. A. Manteuffel, and S. F. McCormick (NASA), pp. 621–634.
[44] J. R. Grace, T. Wairegi, and T. H. Nguyen, "Shapes and velocities of single drops and bubbles moving freely through immiscible liquids," Trans. Inst. Chem. Eng. **54**, 167 (1976).
[45] M. Sussman, A. Almgren, J. Bell, P. Colella, L. Howell, and M. Welcome, "An adaptive level set approach for incompressible two-phase flows," J. Comput. Phys. **148**, 81–124 (1999).
[46] M. Ohta, D. Kikuchi, Y. Yoshida, and M. Sussman, "Robust numerical analysis of the dynamic bubble formation process in a viscous liquid," Int. J. Multiphase Flow **37**, 1059–1071 (2011).
[47] M. Ohta, S. Yamaguchi, Y. Yoshida, and M. Sussman, "The sensitivity of drop motion due to the density and viscosity ratio," Phys. Fluids **22**, 072102 (2010).
[48] M. Jemison, E. Loch, M. Sussman, M. Shashkov, M. Arienti, M. Ohta, and Y. Wang, "A coupled level set-moment of fluid method for incompressible two-phase flows," J. Sci. Comput. (to be published).